Transactions, **SMiRT-26**
Berlin/Potsdam, Germany, July 10-15, 2022
Division III

SPECTRAL EXTRAPOLATION OF FREQUENCY-DEPENDENT FLUIDELASTIC COUPLING COEFFICIENTS FROM CAUSALITY ENFORCING

Jose Antunes[1], Philippe Piteau[2], Xavier Delaune[2], Romain Lagrange[2]

[1] Principal researcher, Centro de Ciências e Tecnologias Nucleares (C2TN), Instituto Superior Técnico (IST), Universidade de Lisboa, 2695-066 Bobadela LRS, Portugal (*jantunes@ctn.tecnico.ulisboa.pt*)
[2] Research Engineer, Université Paris-Saclay, CEA, Service d'Études Mécaniques et Thermiques, F-91191, Gif-sur-Yvette, France

ABSTRACT

Frequency-dependent coupling forces are common in many systems of practical interest, in particular when dealing with flow/structure interactions. The importance of fluidelastic forces in flow-excited vibrations cannot be over-emphasized, in view of their damaging potential. Typically, fluidelastic coupling coefficients are experimentally obtained from vibration experiments, within a limited experimental frequency range. When performing nonlinear time-domain computations, conversion of limited fluidelastic data from the frequency-domain to the time-domain is mandatory, and non-causality will be artificially introduced in the frequency-dependent test data, if one simply assumes that it is nil outside the measured frequency range. Here, a new method is developed for causal frequency interpolation/extrapolation of experimental fluidelastic data. The proposed technique is nonlinear and iterates alternatively between the frequency and time-domains, while enforcing the experimentally available data, as well as causality and regularity conditions, at each iteration. The method is tested and illustrated using as reference data simulated fluidelastic coefficients based on the Granger-Païdoussis model, in the context of heat-exchanger tube bundle vibrations, although the problem addressed embraces a much wider range of applications. The frequency-extended data obtained fulfils the Kramers-Kronig relations and, although unable to recover the dynamical features of the flow-coupling forces which are totally absent from the measured frequency range, the approach has the significant advantage of being model independent and leads to extended data that is regular and physically consistent.

INTRODUCTION

Frequency-dependent coupling forces are common in many systems of practical interest involving interactions between structures and flows or unbounded media, including flow-induced vibrations (FIV) of industrial components (Blevins, 2001), hydroelasticity (Cummins, 1962) and aeroelasticity (Roger, 1977), but also in vibro-acoustics (Axisa and Antunes, 2007) and soil-structure interaction (Wolf and Hall, 1988). When dealing with flow-induced vibrations, the importance of fluidelastic forces can hardly be over-emphasized, in view of their damaging potential. Hence the need for advanced models of fluidelastic coupling, as well as for experimental coupling coefficients, to feed and validate such models. In this work, the problem of fluid-elastic data reduction is revisited in the context of heat-exchanger tube bundle vibrations, although the problem addressed concerns a much wider range of applications.

Typically, as illustrated in Figure 1(a), fluidelastic coupling coefficients are experimentally obtained from vibration experiments performed at various flow velocities and vibration frequencies, see Sawadogo and Mureithi (2014a, 2014b) and Piteau et al. (2018, 2019). Such data are strongly frequency-dependent and, whatever the identification method used, typically confined to a limited experimental

frequency range. This fact becomes problematic when performing nonlinear dynamical analysis of flow-coupled structures, as a conversion of fluidelastic data from the frequency-domain to the time-domain is then mandatory (Piteau et al., 2018). For properly performing such conversion, an extensive frequency range of the flow-coupling coefficients is needed. Otherwise, as will be shown in the following, non-causality will be artificially introduced in the frequency-dependent test data, when computing the inverse FFT of the frequency-dependent test data, for instance if one simply assumes that it is nil outside the measured frequency range. There are several possible strategies to interpolate and extrapolate the fluidelastic data outside the measured frequency range, without violating physics, in particular: (a) Fitting the identified data to a realistic fluidelastic model and then applying time-conversion to the fitted model, as done by Piteau et al. (2018); (b) Implementing interpolation/extrapolation techniques which enforce causality of the frequency-extended data, as well as other possible a priory constraints, a technique suggested by Antunes et al. (2019).

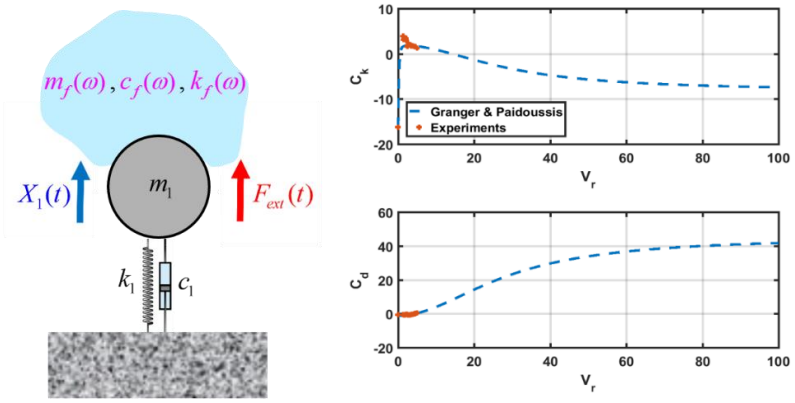

(a) (b)

Figure 1: (a) Conceptual illustration of the identification of fluid-elastic forces; (b) Fitting of experimental fluid-elastic coefficients to the Granger-Païdoussis (1996) model, from Piteau et al. (2018).

As illustrated in Figure 1(b), we have been consistently using the first approach, see Piteau et al. (2018, 2019), by adjusting the experimentally identified flow coefficients (plotted in red) to the Granger-Païdoussis (1996) fluidelastic model (plotted in blue), which is causal by construction. Following our recent work (Antunes et al., 2019), the later approach is further explored in the present paper, where data extrapolation will be addressed without using features connected with any specific theoretical fluid-elastic model, and imposing only a minimum of general physical principles. More specifically, a method is developed for the causal frequency interpolation/extrapolation of experimental fluidelastic or any other frequency-dependent data. The proposed technique is nonlinear and iterates alternatively between the frequency and time-domains, while enforcing causality and other possible a priori established constraints at each iteration. Such approach was inspired by constrained iterative image restoring techniques based on projection onto convex sets (POCS), see Mamonne (1992), although the essential constraint imposed in the present context - causality - is quite distinct from those used for image restoring.

The proposed method is tested and illustrated using simulated fluidelastic coefficients, extracted from the theoretical model developed by Granger and Païdoussis (1996), which is assumed here to supply the reference "experimental data". Actually, at this stage and for validation purposes of the frequency interpolation/extrapolation technique, such approach is more convenient than using actual experimental data, because it give us access to a credible "reality" within an extremely wide frequency range. This illustrative example lays in the context of heat-exchanger tube vibrations, although the problem addressed embraces a much wider range of applications. The frequency-extended data thus obtained also fulfills the Kramers-Kronig relations, see King (2009), which test causality in the frequency domain, while preserving the measured data in the experimental frequency range. As might be expected, the proposed interpolation/extrapolation method cannot recover dynamical features of the flow-coupling forces which are barely reflected on the measured frequency range. Nevertheless, it has the significant advantage of being

model independent and leads to extended data that is regular and physically consistent, therefore usable for the time-domain computations.

FLUID-ELASTIC COUPLING FORCES

Given the basic system shown in Figure 1(a), acted by the external force $F_{ext}(t)$, dynamics may be expressed in the frequency domain as:

$$\left(-\omega^2 m_1 + i\omega c_1 + k_1\right) X_1(\omega) = F_{ext}(\omega) - F_f(\omega) \tag{1}$$

where the flow-coupling force $F_f(\omega)$ is conventionally expressed by:

$$F_f(\omega) = Z_f(\omega) X_1(\omega) \quad \text{with} \quad Z_f(\omega) = -\omega^2 m_f(\omega) + i\omega c_f(\omega) + k_f(\omega) \tag{2}$$

where $Z_f(\omega)$ is a (generalized) "impedance", representative of the flow-coupling. Then, the time-domain fluidelastic force is obtained through the convolution:

$$F_f(t) = \left(z_f * X_1\right)(t) = \int_0^t z_f(\tau)\, X_1(t-\tau)\, d\tau \tag{3}$$

with the fluidelastic impulse function $z_f(t)$ given by the inverse Fourier transform of $Z_f(\omega)$:

$$z_f(t) = \mathcal{F}^{-1}\left[Z_f(\omega)\right] = \frac{1}{2\pi} \int_{-\infty}^{\infty} Z_f(\omega)\, e^{i\omega t} d\omega \tag{4}$$

The integral in expression (4) shows that, for an adequate time-domain representation of the fluidelastic impulse function $z_f(t)$, the impedance $Z_f(\omega)$ *must be known over an extended frequency range*, otherwise, unacceptable artefacts will arise. In particular, non-causality will be introduced if one simply assumes that $Z_f(\omega)$ is nil outside the measured frequency range.

PROPOSED INTERPOLATION/EXTRAPOLATION TECHNIQUE

Causality

Causality of the fluidelastic forces is an essential physical constraint, which universally applies, whatever the actual form of any specific flow force. Then. it is tempting to use such feature when developing a tentative "reconstruction" scheme for $Z_f(\omega)$, outside the measured range $[\omega_{\min}\ \omega_{\max}]$. Such a method will be developed in the following sections. Causality means that the system response cannot precede the excitation. It can be defined in two basic manners, according to the physical domain of interest. In the *time domain*, causality is simply stated as:

$$z_f(t) = 0 \quad \text{for} \quad t < 0 \tag{5}$$

while in the *frequency domain*, causality of linear systems is expressed in terms of the so-called Cramers-Kronig relations, see Kramers (1927) and Kronig (1926), which relate the real and imaginary parts of $Z_f(\omega) = Z_R(\omega) + i\, Z_I(\omega)$:

$$\begin{cases} Z_R(\omega) = \mathcal{H}\left[Z_I(\omega)\right] = \dfrac{1}{\pi}\mathcal{P} \displaystyle\int_{-\infty}^{\infty} \frac{Z_I(\varpi)}{\varpi - \omega} d\varpi = \frac{1}{\pi}\mathcal{P} \int_0^{\infty} \frac{\varpi Z_I(\varpi)}{\varpi^2 - \omega^2} d\varpi \\ Z_I(\omega) = -\mathcal{H}\left[Z_R(\omega)\right] = -\dfrac{1}{\pi}\mathcal{P} \displaystyle\int_{-\infty}^{\infty} \frac{Z_R(\varpi)}{\varpi - \omega} d\varpi = -\frac{\omega}{\pi}\mathcal{P} \int_0^{\infty} \frac{Z_R(\varpi)}{\varpi^2 - \omega^2} d\varpi \end{cases} \tag{6}$$

where $\mathcal{H}\left[X(\omega)\right]$ stands for the Hilbert transform of $X(\omega)$, with $\mathcal{P}$ denoting the Cauchy principal value of the improper integrals (which display a singularity at $\varpi = \omega$) and, for their convergence, it is assumed that $Z_f(\omega \to \infty) \to 0$. From (6) stems that the causality of linear systems imposes precise relations between the conservative and dissipative terms of $Z_f(\omega)$, which is a very interesting (and even surprising) feature, as the physical mechanisms related to them are typically quite distinct.

Basic reconstruction algorithm

Several numerical schemes may be developed based on the causality relations (5) and/or (6). In the present work we propose a nonlinear method for the causal frequency interpolation/extrapolation of experimental fluidelastic data, which iterates alternatively between the frequency and time-domains, while enforcing causality and other possible a priori established constraints at each iteration. Our approach may be rooted to the seminal work by Gerchberg (1974) and Papoulis (1975), which led to the POCS-type constrained iterative image restoring techniques, see Mammone (1992), mentioned in the introduction.

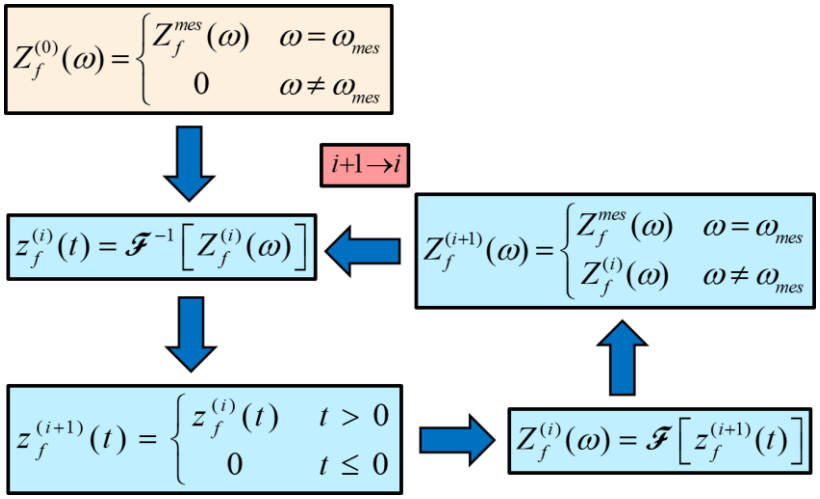

Figure 2. Proposed iterative interpolation/extrapolation of the fluidelastic data.

The basic reconstruction scheme developed here is shown in Figure 2, for a generic causal function $Z_f(\omega)$, with the corresponding time-domain representation $z_f(t) = \mathcal{F}^{-1}\left[Z_f(\omega)\right]$. In summary:

(a) An initial impedance function $Z_f^{(0)}(\omega)$ is built from the frequency-bounded experimental data $Z_f^{mes}(\omega)$, by zeroing the unknown data in the unmeasured frequency range;

(b) An iterative scheme is built, by alternating estimations in the frequency domain $Z_f^{(i)}(\omega)$ and in the time domain $z_f^{(i)}(t)$, using the direct and inverse Fourier transforms;

(c) A nonlinear function reconstruction is obtained at each iteration, by imposing the measured data on $Z_f^{(i)}(\omega)$ within the identified frequency range, while imposing causality in the time domain by zeroing $z_f^{(i)}(t)$ for $t < 0$.

In general, for M constraining POCS linear or nonlinear constraints, the feature projections (c) - here denoted $P_m \otimes \equiv P_m(\otimes)$, with $m = 1, 2, \cdots, M$ - may be fully enforced through the following recursions, see Opial (1967), Gubin et al. (1967), Youla and Webb (1982) and Sezan and Stark (1982):

$$z_f^{(i+1)}(t) = P_M P_{M-1} \cdots P_2 P_1 \, z_f^{(i)}(t) \tag{7}$$

As can be formally demonstrated (Youla and Webb, 1982), POCS-type algorithms converge to a unique solution, whatever the initial conditions of the nonlinear iterative scheme. Moreover, it will also be shown that the proposed reconstruction method is quite robust to noise and/or errors in the measured data. These are two important and useful properties of the proposed data interpolation/extrapolation method.

APPLICATION TO THE GRANGER-PAÏDOUSSIS FLUIDELASTIC MODEL

Before the present application to fluidelastic forces, as a preliminary step, we asserted the behavior of the proposed interpolation/extrapolation approach on a basic system, consisting of a single degree of freedom main structure with a coupled oscillator, providing an additional "pseudo-flow" degree of freedom. Interpolations/extrapolations were achieved, ranging from moderately to extremely successful, depending on the frequency range of the "measured" data used. These preliminary explorations also confirmed that the proposed data reconstruction technique is robust to noise and immune to the initialization conditions of the iterative scheme.

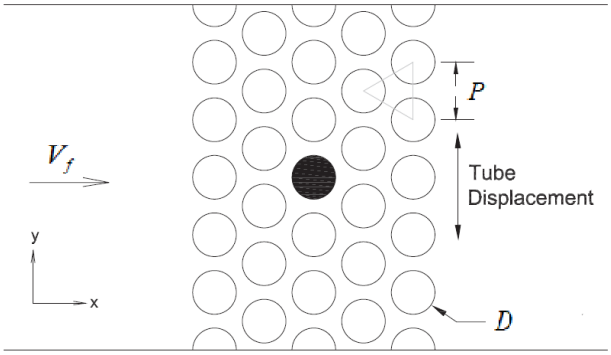

Figure 3: Flexible tube in a rigid normal triangular bundle, subjected to cross-flow and vibrating along the lift direction, adapted from Mahon and Meskell (2009).

Turning now to fluidelastic forces, the theoretical "quasi-unsteady" fluidelastic model of Granger and Païdoussis (1996) will be used here, for its convenience and physical insight. We considering a single flexible tube within a rigid bundle, which is subjected to cross-flow and vibrates along the lift direction, as shown in Figure 3. The tubes have diameter D and immersed length L, the bundle pitch ratio is P/D, the fluid has density ρ_f and pitch velocity V_f. The tube lift vibration is denoted $Y(t)$. In the time domain, the Granger-Païdoussis (1996) model leads to the fluidelastic lift force:

$$F_f(\bar{t}) = \frac{1}{2}\rho_f V_f^2 LD\left[\frac{\partial C_L}{\partial \bar{y}}\left(g(\bar{t}) * \frac{Y(\bar{t})}{D}\right) - C_D \frac{\dot{Y}(\bar{t})}{V_f}\right] \tag{8}$$

which does not include the fluid inertia term, as the added mass is assumed to be flow-independent and encapsulated with the structural mass. In formulation (8) the dimensionless time $\bar{t} = tV_f / D$ and space $\bar{y} = y/D$ are used, as well as the steady drag and lift flow force coefficients C_D and C_L. Finally, a motion-to-force delay term is incorporated through a convolution of the tube displacement with the following *flow relaxation ("memory") function*:

$$g(\bar{t}) = \frac{d\Phi(\bar{t})}{d\bar{t}} \quad \text{with} \quad \Phi(\bar{t}) = \left(1 - \sum_{p=1}^{P} \alpha_p \, e^{-\beta_p \bar{t}}\right) \mathcal{H}(\bar{t}) \tag{9}$$

where α_p and β_p (with $p = 1, 2, \cdots, P$) are experimental parameters of the exponential relaxation describing flow convection-diffusion adjustment processes. From (9) we obtain:

$$g(\bar{t}) = \left(\sum_{p=1}^{P} \alpha_p \beta_p \, e^{-\beta_p \bar{t}} \right) \mathcal{H}(\bar{t}) + \left(1 - \sum_{p=1}^{P} \alpha_p e^{-\beta_p \bar{t}} \right) \delta(\bar{t}) \tag{10}$$

and the corresponding frequency domain function is:

$$G(\bar{\omega}) = \mathcal{F}\left[g(\bar{t}) \right] = \sum_{p=1}^{P} \frac{\alpha_p \beta_p}{\beta_p + i\bar{\omega}} + \left(1 - \sum_{p=1}^{P} \alpha_p \right) = 1 - i\bar{\omega} \sum_{p=1}^{P} \frac{\alpha_p}{\beta_p + i\bar{\omega}} \tag{11}$$

From (8) and (11), one obtains the dimensionless flow-coupling impedance, see Piteau et al. (2018):

$$\bar{Z}_f(\bar{\omega}) = \frac{Z_f(\bar{\omega})}{(1/2)\rho_f V_f^2 L} = \frac{\partial C_L}{\partial \bar{x}} \left(1 - i\bar{\omega} \sum_{p=1}^{P} \frac{\alpha_p}{\beta_p + i\bar{\omega}} \right) - i\bar{\omega} C_D \tag{12}$$

and the corresponding dimensionless impulse function:

$$\bar{z}_f(\bar{t}) = \frac{z_f(\bar{t})}{(1/2)\rho_f V_f^2 L} = \frac{\partial C_L}{\partial \bar{x}} g(\bar{t}) - C_D \dot{\delta}(\bar{t}) \tag{13}$$

with $g(\bar{t})$ given by (10). The dimensionless coefficients $\partial C_L / \partial \bar{x}$ and C_D in (12) and (13) can be inferred from the data by Granger and Païdoussis (1996), based on experiments by Price and Païdoussis (1986). For a *normal triangular array*:

$$\frac{\partial C_L}{\partial \bar{x}} = -19.2\, c^2 \quad ; \quad C_D = 3.8\, c^2 \quad \text{with} \quad c = \frac{V_\infty}{V_f} = \frac{P/D - 1}{P/D} \tag{14}$$

The parameters used in the following are those found by Meskell (2009) using a single-term in the series model (12), with $\alpha_1 = 1$, $\beta_1 = 0.157$ and the coefficients $\partial C_L / \partial \bar{x} = -2.13$ and $C_D = 0.422$ computed from (14), for a *normal triangular array* with $P/D = 1.375$ (note that the values $\partial C_L / \partial \bar{x} = -10.15$ and $C_D = 2.01$ given by Meskell (2009) are erroneous, because of a wrong correction factor $c = V_\infty / V_f$ used there). In addition, in his analysis of the relaxation function $g(\bar{t})$, Meskell (2009) argues that physics prevent an impulse at $\bar{t} = 0$ for flow-excited tubes: *"It should be noted that at time* $\tau = 0$ *the tube has not experienced any displacement, thus the lift and the circulation, and hence the memory function, should be zero"*. Then, the constraint $\sum_{p=1}^{P} \alpha_p = 1$ is extracted from equation (10), when zeroing the impulse term at $\bar{t} = 0$. The fluidelastic impedance (12) then reads:

$$\bar{Z}_f(\bar{\omega}) = \frac{Z_f(\bar{\omega})}{(1/2)\rho_f V_f^2 L} = \frac{\partial C_L}{\partial \bar{x}} \sum_{p=1}^{P} \frac{\alpha_p \beta_p}{\beta_p + i\bar{\omega}} - i\bar{\omega} C_D \quad \text{with} \quad \sum_{p=1}^{P} \alpha_p = 1 \tag{15}$$

Looking at equation (15), one notices that $\bar{Z}_f(\bar{\omega})$ displays terms of profoundly different nature:

(a) All P terms of the series tend to α_p when $\bar{\omega} \to 0$ and to zero when $\bar{\omega} \to \infty$, in accordance with the classic structure of these terms, all of them being *strictly proper*. The impulse response component stemming from these terms is well behaved, of decreasing exponential nature, see equation (10).

(b) On the contrary, the last term $-i\bar{\omega} C_D$ is obviously *improper*. Because energy will increase unbounded with frequency, this derivative operator will lead to a problematic singularity at $\bar{t} = 0$, see equation (13).

The P terms (a) dominate $\bar{Z}_f(\bar{\omega})$ at lower frequencies, while the derivative term (b) controls the behavior of $\bar{Z}_f(\bar{\omega})$ at higher frequencies. In order to bypass the difficulty connected with the improper nature of (15), we address the problem by separating $\bar{Z}_f(\bar{\omega})$ into two parts, the first strictly proper and the

second improper. Actually, following the theoretical rationale presented by Antunes et al. (2022), for any given flow velocity the fluidelastic forces can in general be expressed as:

$$\bar{Z}_f(\bar{\omega}) = \sum_{p=1}^{P} \frac{R_p}{\lambda_p + i\bar{\omega}} + \bar{\omega}^2 M + i\bar{\omega}C + K \tag{16}$$

where the basic series has P strictly proper terms and, additionally, one considers up to three "pure" (not frequency-dependent) improper terms, respectively of inertia, dissipation and stiffness nature. Because the reference added mass term is typically associated to the structural mass, we drop it from (16), hence:

$$\bar{Z}_f(\bar{\omega}) = \sum_{p=1}^{P} \frac{R_p}{\lambda_p + i\bar{\omega}} + i\bar{\omega}C + K = \bar{W}_f(\bar{\omega}) + i\bar{\omega}C + K \quad \Rightarrow \quad \begin{cases} \mathrm{Re}\left[\bar{Z}_f(\bar{\omega})\right] = \mathrm{Re}\left[\bar{W}_f(\bar{\omega})\right] + K \\ \mathrm{Im}\left[\bar{Z}_f(\bar{\omega})\right] = \mathrm{Im}\left[\bar{W}_f(\bar{\omega})\right] + \bar{\omega}C \end{cases} \tag{17}$$

Therefore, given some bandlimited fluidelastic data $\bar{Z}_f(\bar{\omega})$, if we can isolate the improper terms pertaining to the coefficients C and K, we are then left with a strictly proper and well behaved function $\bar{W}_f(\bar{\omega})$, which can be causally extrapolated using the iterative projection technique developed. The simultaneous identification of C, K and $\bar{W}_f(\bar{\omega})$ from $\bar{Z}_f(\bar{\omega})$ is not an obvious task. Here we adopted the following strategy:

1) Define plausible exploration ranges for $C_{\min} \le C^{(j)} \le C_{\max}$ and $K_{\min} \le K^{(j)} \le K_{\max}$;

2) For each tentative values of $C^{(j)}$ and $K^{(j)}$, compute $\bar{W}_f^{(j)}(\bar{\omega})$ from $\bar{Z}_f(\bar{\omega})$ using (17);

3) Interpolate/extrapolate the experimental data of $\bar{W}_f^{(j)}(\bar{\omega})$ using the proposed technique;

4) Compute the impulse response $\bar{w}_f^{(j)}(\bar{t})$ from the extrapolated $\bar{W}_f^{(j)}(\bar{\omega})$ estimation;

5) Define a "pulse-index" value $P(j) = \bar{w}_f^{(j)}(0)$ of the $\bar{w}_f^{(j)}(\bar{t})$ estimation;

6) Because the true $\bar{W}_f(\bar{\omega})$ is strictly proper, then the true $\bar{w}_f(\bar{t})$ is not impulsive, which implies the optimality condition for identifying the "true" C, K and $\bar{W}_f(\bar{\omega})$:

$$\begin{cases} C^{(j_{opt})} = C \\ K^{(j_{opt})} = K \end{cases} \Rightarrow \begin{cases} \bar{W}_f^{(j_{opt})}(\bar{\omega}) = \bar{W}_f(\bar{\omega}) \\ \bar{w}_f^{(j_{opt})}(\bar{t}) = \bar{w}_f(\bar{t}) \end{cases} \Rightarrow \quad j_{opt} \quad \text{such that} \quad P(j_{opt}) = \min\left(P(j)\right) \tag{18}$$

This scheme can be implemented using either a systematic exploration of $C_{\min} \le C^{(j)} \le C_{\max}$ and $K_{\min} \le K^{(j)} \le K_{\max}$, or else using an optimization algorithm for faster convergence. Here, we pragmatically postulate that $K = 0$ (which is true for the Granger-Païdoussis model, although not in general) and systematically explore C in the range $0 \le C^{(j)} \le 5C_D$, see equations (15) and (17), for the single-term Meskell (2009) approximation polluted with 10% errors (e.g., 10% of the $\bar{Z}_f(\bar{\omega})$ rms value in the measured frequency range).

We now assume that the data $\bar{Z}_f(\bar{\omega})$ was "measured" in the lower frequency range $0 \le \bar{\omega} \le 1$. Figure 4 shows the reference (green) and the band-limited "measured" (red) data, at the start of the iterative procedure, when zero values are enforced in the non-measured frequency range. The corresponding proper function $\bar{W}_f(\bar{\omega}) = \bar{Z}_f(\bar{\omega}) - i\bar{\omega}C^{(j_{opt})}$, obtained after the optimally identified estimation of C is shown in Figure 5. One can notice that $\bar{W}_f(\bar{\omega}) \to 0$ as $\bar{\omega} \to \infty$, a compulsory property of strictly proper functions. The last plot of Figure 5 presents the initial estimate of the corresponding impulse function $\bar{w}_f(\bar{t})$, showing that at this stage the model is not causal.

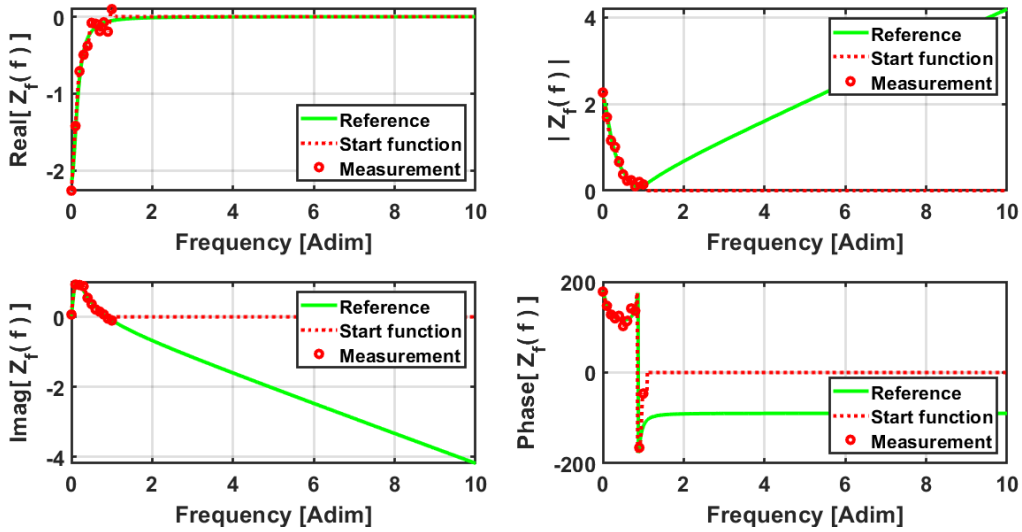

Figure 4: Fluidelastic impedance $\bar{Z}_f(\bar{\omega})$ from the Granger-Païdoussis model, for a normal triangular array with $P/D = 1.375$, using parameters $\alpha_1 = 1$, $\beta_1 = 0.157$, $\partial C_L / \partial \bar{x} = -2.13$ and $C_D = 0.422$, with experimental data provided in the frequency range $0 \le \bar{\omega} \le 1$ with 10% error: Initial approximation with zeroed unmeasured frequency range.

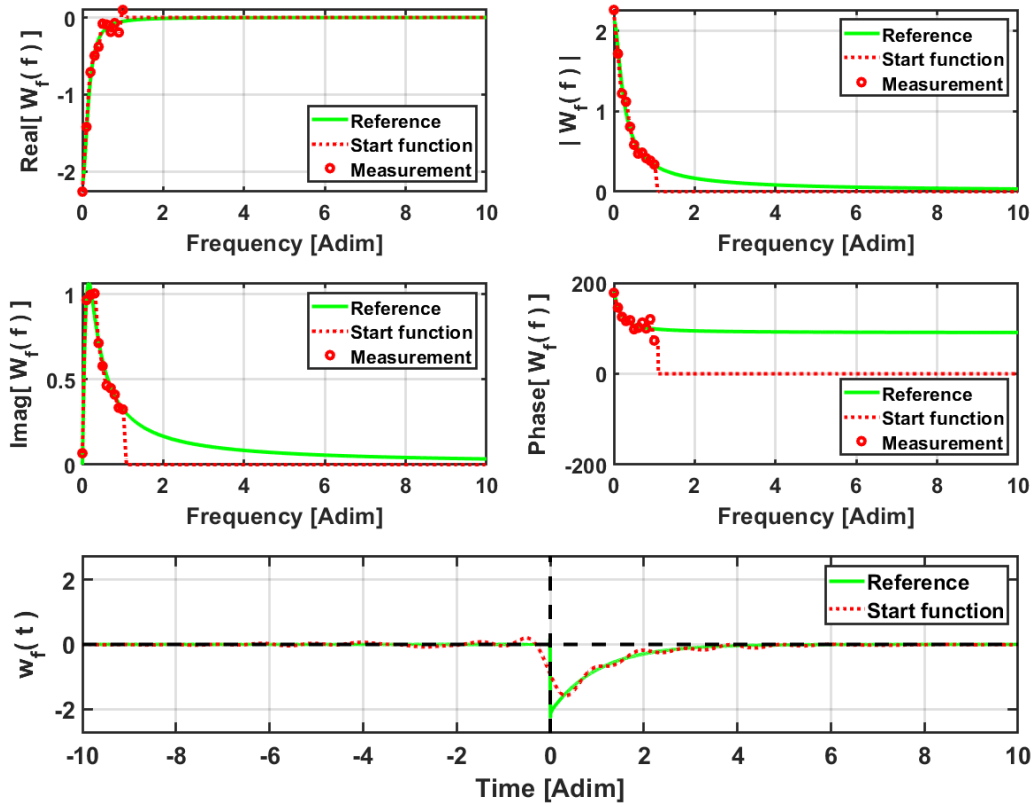

Figure 5: Derived proper functions $\bar{W}_f(\bar{\omega})$ and $\bar{w}_f(\bar{t})$, from the Granger-Païdoussis model, for a normal triangular array with $P/D = 1.375$, using parameters $\alpha_1 = 1$, $\beta_1 = 0.157$, $\partial C_L / \partial \bar{x} = -2.13$ and $C_D = 0.422$, with experimental data provided in the frequency range $0 \le \bar{\omega} \le 1$ with 10% error: Initial approximation with zeroed unmeasured frequency range.

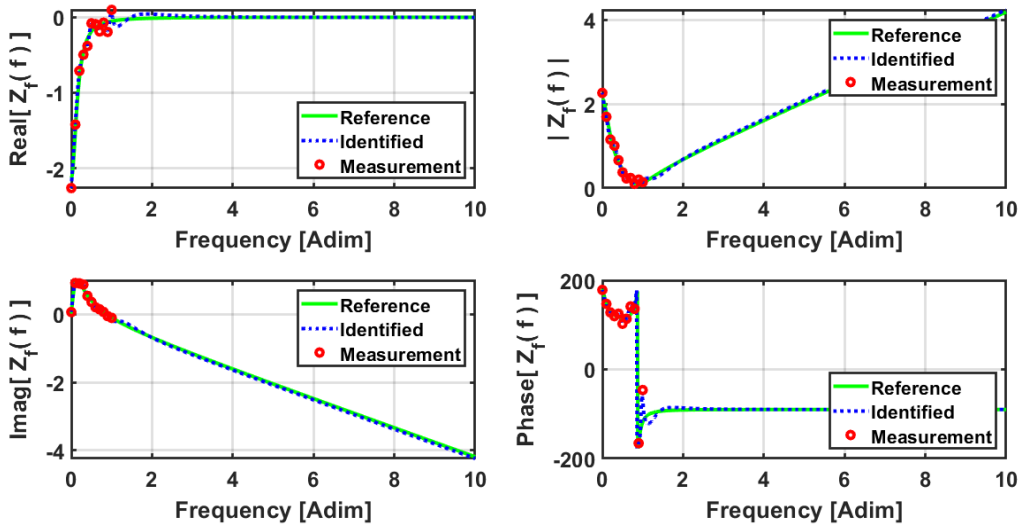

Figure 6: Fluidelastic impedance $\bar{Z}_f(\bar{\omega})$ from the Granger-Païdoussis model, for a normal triangular array with $P/D = 1.375$, using parameters $\alpha_1 = 1$, $\beta_1 = 0.157$, $\partial C_L / \partial \bar{x} = -2.13$ and $C_D = 0.422$, with experimental data provided in the frequency range $0 \le \bar{\omega} \le 1$ with 10% error: Final data extrapolation after 10000 iterations.

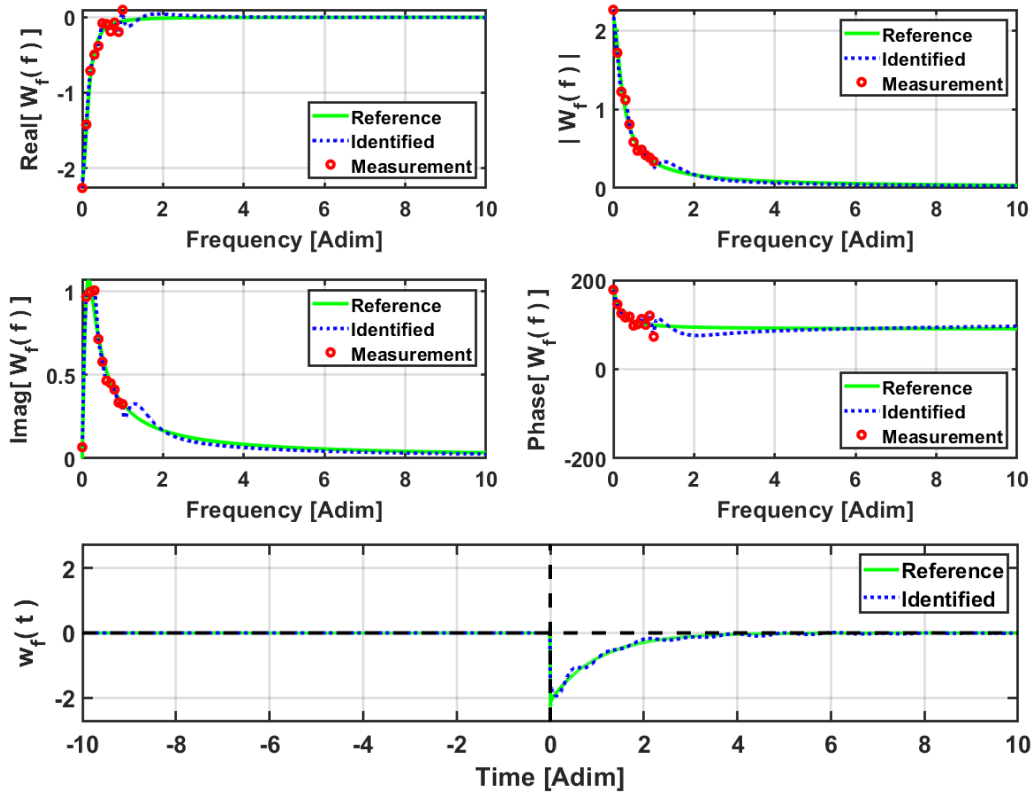

Figure 7: Derived proper functions $\bar{W}_f(\bar{\omega})$ and $\bar{w}_f(\bar{t})$, from the Granger-Païdoussis model, for a normal triangular array with $P/D = 1.375$, using parameters $\alpha_1 = 1$, $\beta_1 = 0.157$, $\partial C_L / \partial \bar{x} = -2.13$ and $C_D = 0.422$, with experimental data provided in the frequency range $0 \le \bar{\omega} \le 1$ with 10% error: Final data extrapolation after 10000 iterations.

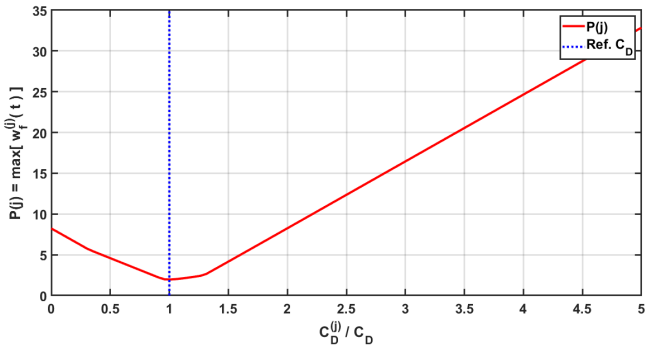

Figure 8: Computation of the "pulse index" $P(j)$ of $\bar{w}_f^{(j)}(\bar{t})$, as a function of $C^{(j)}$.

Figure 6 shows the extrapolated fluidelastic impedance $\bar{Z}_f(\bar{\omega}) = \bar{W}_f(\bar{\omega}) + i\bar{\omega}C^{(j_{opt})}$, obtained from the extrapolated causal function $\bar{W}_f(\bar{\omega})$ shown in Figure 7, which also presents the corresponding impulse function $\bar{w}_f(\bar{t})$, these results being now clearly causal. All these extrapolated estimations closely follow the reference results of the Granger-Païdoussis model, in a satisfying manner.

Finally, Figure 8 presents the "pulse-index" function $P(j)$ as a function of $C^{(j)}/C$, confirming that - as was logically assumed - $P(j)$ displays a minimum for the true value $C^{(j_{opt})}/C = 1$. Therefore, the proposed identification scheme indeed leads to a correct estimation of the improper term coefficient C.

CONCLUSION

In this work, we proposed a new approach for the frequency interpolation and extrapolation of experimental fluidelastic data. The technique iterates between the frequency and the time-domain, where the measured data and the physical causality (and, eventually, other a priori known features) are respectively enforced. Additionally, an optimization scheme was also developed in order to separate the fluidelastic data into its strictly proper and improper components. Then, the iterative interpolation/extrapolation method is applied to the well-behaved proper part, which is later added to the impulsive improper part.

The proposed technique was applied to simulated fluidelastic data, stemming from the Granger-Païdoussis model. Overall, the obtained results are quite encouraging, and suggest that the proposed approach is usable for actual experimental data. However, not surprisingly, the effectiveness of the obtained interpolated/extrapolated estimations is heavily dependent on the physical relevance of experimental data processed. Typically, experimental data pertaining to dynamically relevant frequency ranges lead to excellent interpolation/extrapolation reconstructions, while the use of experimental data from less relevant frequency ranges can miss significant dynamical features. The proposed data-extension approach has room for improvements, namely by devising new a priori known features of the coupling impedance to enforce, beyond the causality and smoothness properties used here.

REFERENCES

Antunes, J., Piteau, P., Delaune, X. and Lagrange, R. (2019). “Estimation of frequency-dependent fluidelastic coupling coefficients over untested frequency ranges for performing time-domain analysis”, *IUTAM Symposium on Fluid-Structure Interaction*, Montreal, Canada, August 12-15.

Antunes, J., Piteau, P., Delaune, X. and Lagrange, R. (2022). “Frequency-independent modelling of experimental fluidelastic forces using hidden flow variables”, *12th International Conference on Flow-Induced Vibration (FIV-2022)*, Paris-Saclay, France, July 5-8.

Axisa, F. and Antunes, J. (2007). *Modelling of mechanical systems: Fluid-structure interaction*, Elsevier, ISBN: 0-7506-6847-4.

Blevins, R. D. (2001). *Flow-induced vibration*, Krieger Publishing Co., ISBN: 1-57524-183-8.

Cummins, W. E. (1962). "The impulse response function and ship motions", *Schiffstechnik*, 9, 101-109.

Gerchberg, R. W. (1974). Super-resolution through error energy reduction, *Optica Acta*, 21, 709-720.

Gomez, C., Bunks, C., Chancelier, J.-P., Delebecque, F., Goursat, M., Nikoukhah, R. and Steer, S. (1999). *Engineering and scientific computing with Scilab*, Springer, ISBN: 978-1-4612-7204-5.

Granger, S. and Païdoussis, M. (1996). "An improvement to the quasi-steady model with application to cross-flow-induced vibration of tube arrays", *Journal of Fluid Mechanics*, 320, 163-184.

Gubin, L. G., Polyak, B. T. and Raik, E. V. (1967). "The method of projections for finding the common point of convex sets", *USSR Computational Mathematics and Mathematical Physics*, 7, 1-24.

Gur, E. and Zalevsky, Z. (2007). "Single-image digital super-resolution: A revised Gerchberg-Papoulis algorithm", *IAENG International Journal of Computer Science*, 34, Paper IJCS-34-2-14.

King, F. W. (2009). *Hilbert transforms*. Cambridge University Press, ISBN 978-0-521-51720-1.

Kramers, H. A. (1927). "La diffusion de la lumière par les atomes", *Atti del Congresso Internationale dei Fisici - Transactions of Volta Centenary Congress*, 2, 545-557.

Kronig, R. (1926). "On the theory of the dispersion of X-rays", *Journal of the Optical Society of America*, 12, 547-557.

Mahon, J. and Meskell, C. (2009). "Surface pressure distribution survey in normal triangular tube arrays", *Journal of Fluids and Structures*, 25, 1348-1368.

Mammone, R. J. (1992). *Computational methods of signal recovery and recognition*, Wiley-Interscience, ISBN 978-0471853848.

Meskell, C. (2009). "A new model for damping controlled fluidelastic instability in heat ex-changer tube arrays", *Proceedings of IMechE A: Journal of Power and Energy*, 223, 361-368.

Opial, Z. (1967). "Weak convergence of the sequence of successive approximations for nonexpansive mappings", *Bulletin of the American Mathematical Society*, 73, 591-597.

Papoulis, A. (1975) "A new algorithm in spectral analysis and band-limited extrapolation", *IEEE Transaction on Circuits and Systems*, 19, 735-742.

Piteau, P., Borsoi, L., Delaune, X. and Antunes, J. (2018). "Time-domain numerical simulations of a loosely supported tube subjected to frequency-dependent fluid-elastic forces", *Journal of Fluids and Structures*, 81, 383-398.

Piteau, P., Delaune, X., Borsoi, L. and Antunes, J. (2019). "Experimental identification of the fluid-elastic coupling forces on a flexible tube within a rigid square bundle subjected to single-phase cross-flow", *Journal of Fluids and Structures*, 86, 156-169.

Price, S. and Païdoussis, M. (1986). "A single-flexible-cylinder analysis for the fluidelastic instability of an array of flexible cylinders in cross-flow", *ASME Journal of Fluids Engineering*, 108, 193-199.

Roger, K. L. (1977). "Airplane math modelling methods for active control design", *Proc. AGARD-CP-228*.

Savitzky, A. and Golay, M. J. (1964). "Smoothing and differentiation of data by simplified least squares procedures", *Analytical Chemistry*, 36, 1627-1639.

Sawadogo, T. and Mureithi, N. (2014a). "Fluid-elastic instability study in a rotated triangular tube array subject to two-phase cross-flow. Part 1: Fluid force measurements and time delay extraction", *Journal of Fluids and Structures*, 49, 1-15.

Sawadogo, T. and Mureithi, N. (2014b). "Fluid-elastic instability study in a rotated triangular tube array subject to two-phase cross-flow. Part 2: Experimental tests and comparison with theoretical results", *Journal of Fluids and Structures*, 49, 16-28.

Sezan, M. I. and Stark, H. (1982). "Image restoration by the method of convex projections: Part 2 - Applications and numerical results", *IEEE Transactions on Medical Imaging*, 1, 95-101.

Sezan, M. I. and Stark, H. (1983). "Image restoration by convex projections in the presence of noise", *Applied Optics*, 22, 2781-2789.

Wolf, J. and Hall, W. (1988). *Soil-structure-interaction analysis in time domain*, Prentice-Hall, ISBN: 0-13-822974-0.

Youla, D. C. and Webb, H. (1982). "Image restoration by the method of convex projections: Part 1 - Theory", *IEEE Transactions on Medical Imaging*, 1, 81-94.